Geoderma 472 (2026) 117908

Contents lists available at ScienceDirect

Geoderma

journal homepage: www.elsevier.com/locate/geoderma

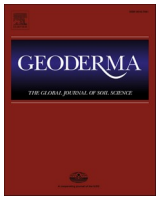

Effect of wind-driven rain on soil erosion processes under different soil surface roughness conditions

Sophia Bahddou [a,b,c,1,*], Wilfred Otten [a], W. Richard Whalley [b], Ho-Chul Shin [b], Mohamed El Gharous [c], Adnane Beniaich [c], Hannah V. Cooper [b,d], R. Jane Rickson [a]

[a] Faculty of Engineering and Applied Sciences, Cranfield University, Cranfield, Bedfordshire MK43 0AL, United Kingdom
[b] Sustainable Soils and Crops Strategic Area, Rothamsted Research, West Common, Harpenden, Hertfordshire AL5 2JQ, United Kingdom
[c] Agricultural Innovation and Technology Transfer Center (AITTC), College of Agriculture and Environmental Science, Mohammed VI Polytechnic University (UM6P), Ben Guerir 43150, Morocco
[d] School of Biosciences, The University of Nottingham, Sutton Bonington, Nottinghamshire LE12 5RD, United Kingdom

ARTICLE INFO

Handling Editor: Dr. H. Neely

Keywords:
Rainfall erosivity
Rainfall simulator
Runoff
Soil loss
Splash erosion
Wind-driven rain
Wind simulator

ABSTRACT

Soil erosion is a critical issue that threatens agricultural productivity and long-term sustainability. While the effects of wind and rainfall on soil erosion are often studied separately, their combined effects on hydrological and erosion processes, under varying soil surface conditions, remain poorly explored. Understanding erosion dynamics requires evaluating the interactions between water, wind, and soil properties. Therefore, this study investigated the effect of windless rain (WLR) and wind-driven rain (WDR) at varying wind velocities on runoff, infiltration, and soil loss (through runoff and splash erosion) on both smooth and rough soil surfaces using a novel setup comprising rainfall and wind simulators. The study also quantified the effect of different rainfall events on soil surface roughness (SSR). Findings indicate that WDR significantly accelerated runoff generation and produced higher runoff volume and soil loss compared to WLR, due to increased rainfall kinetic energy caused by wind velocity. On smooth surfaces under the highest wind velocity, WDR increased runoff volume, sediment load, and sediment concentration by 74 %, 43 %, and 143 %, respectively, compared to WLR. Rough surfaces mitigated these effects at lower wind velocities but were less effective under higher wind speeds, resulting in soil and water losses comparable to or exceeding those measured under WLR. Moreover, WDR increased SSR on smooth surfaces by up to 172 % but reduced it on rough surfaces by up to 30 %. These results demonstrate that wind increases rainfall erosivity, affecting soil erosion processes. However, the magnitude of this effect was also influenced by wind velocity and initial SSR. Therefore, incorporating these factors is crucial for accurately assessing soil and water losses in erosion studies.

1. Introduction

Soil erosion involves the detachment, entrainment, transport and deposition of soil particles, often accelerated by erosive agents such as water and wind. Climate change is anticipated to exacerbate soil erosion by increasing the frequency and intensity of extreme weather events, such as heavy rainfall, droughts and strong winds (Bolan et al., 2024). In the case of soil erosion by water, raindrop impact and surface runoff play crucial roles as the primary erosive forces (Kinnell, 2005). When soil erosion is caused by wind, the erosion rate is influenced by wind velocity (Zhang et al., 2019). The simultaneous action of wind and water during natural rainstorms can lead to accelerated soil erosion rates, especially in arid and semi-arid regions (Visser et al., 2004). However, most erosion studies have evaluated the individual effects of erosive agents.

There has been a growing interest in soil erosion arising from the combined effects of wind and water (An et al., 2023). A positive relationship was found between wind velocity and soil erosion rates during a rainfall event (Erpul et al., 2003a; Mahmoodabadi et al., 2021). Wind may enhance detachment and transport of soil particles by increasing both the kinetic energy (KE) and incident impact angle of raindrops

* Corresponding author at: Agricultural Innovation and Technology Transfer Center (AITTC), College of Agriculture and Environmental Science, Mohammed VI Polytechnic University (UM6P), Ben Guerir 43150, Morocco.
E-mail address: sophia.bahddou@um6p.ma (S. Bahddou).
[1] https://orcid.org/0000-0002-4097-1237.

https://doi.org/10.1016/j.geoderma.2026.117908
Received 25 March 2025; Received in revised form 4 June 2026; Accepted 18 June 2026
Available online 23 June 2026
0016-7061/© 2026 The Authors. Published by Elsevier B.V. This is an open access article under the CC BY license (http://creativecommons.org/licenses/by/4.0/).

(Erpul et al., 2005; 2013; Iserloh et al., 2013; Marzen et al., 2016; Arshad et al., 2019). These effects are related to wind velocity. Helming (2001) found that at the highest wind velocity (10.5 m s^{-1}), rainfall KE could be 3.5 times higher than in windless conditions. Furthermore, after a raindrop impact detaches and propels soil particles and/or micro-aggregates into the airflow, the wind can carry these dislodged particles up to 3 m in rain driven by wind velocities of 6 m s^{-1}, and up to 6 m in rain driven by wind velocities of 10 and 12 m s^{-1} (Erpul et al., 2002), but these trajectories depend on the mass and density of the soil particle. Few studies have measured the vertical profile of entrained soil particles, including the bedload and suspended particles eroded due to wind-driven rain (WDR). In addition to that, the simultaneous assessment of hydrological responses (i.e. runoff and infiltrate volumes) and soil loss, particularly splash erosion, under wind-driven rain conditions received little attention in previous erosion studies and represents an important research need.

Soil and water losses caused by WDR appear to be influenced not only by the wind-imparted modifications to raindrops and shallow surface runoff, but also significantly affected by other variables related to soil surface attributes (Ries et al., 2014), notably soil surface roughness (SSR). In situations where rain is driven by wind, the influence of soil properties may be more significant compared to conditions without wind, due to the additional effect of profile wind drag (Marzen et al., 2015).

Bahddou et al. (2023) have shown that SSR affects runoff initiation time during a rainfall event, total runoff volume, sediment load and the amount of rainsplash erosion. The authors also showed that erosive forces altered the roughness of the soil surface. Previous research found that SSR of initially rough surfaces decreases due to the rainfall KE breaking down soil aggregates and ridges (da Rocha Junior et al., 2016; Bahddou et al., 2023). On the other hand, smooth soil surfaces become rougher after a rainfall event due to detachment of soil particles caused by the raindrop impact (Bahddou et al., 2023) and micro-rill development on the soil surface (Huang & Bradford, 1992; Römkens et al., 2001). However, these studies only considered the rainfall event although, in reality, wind and rainfall act together on erosion processes.

The aim of this study is to gain a key mechanistic insight into the hydrological and erosional responses of soils under windless rain (WLR) and WDR. The objectives of this research are to a) compare the effects of WLR and WDR (i) on surface runoff and infiltrate volumes, and (ii) on soil loss due to runoff and rainsplash erosion; b) compare the effects of surface roughness (i.e. smooth and rough surfaces) on soil and water losses under WLR and WDR events; and c) study the changes in surface roughness (i.e. smooth and rough surfaces) under the different erosive events. We hypothesise that the interaction of wind with falling raindrops would increase rainfall erosivity leading to increased soil detachment and transport, as well as a more pronounced change in the initial SSR.

2. Materials and methods

2.1. Preparation of erosion trays

Soil erosion trays were prepared following the methodology described in Bahddou et al. (2023). An air-dried sandy loam soil (16 % clay, 28 % silt and 56 % sand) was sieved through a 4 mm mesh screen and packed into soil erosion trays of 50 cm length, 25 cm width and 8.5 cm depth. Each tray was filled with 15 kg of sieved soil and packed in five successive horizontal layers. Each layer was compacted manually using a flat soil packer by applying repeated static pressure to achieve a uniform bulk density of 1.4 g cm^{-3} throughout the profile. The trays were filled up with soil to the level of a V-shaped runoff outlet from which runoff samples (along with any eroded soil in the runoff) would be collected during the rainfall event. An additional layer of soil was added and graded to the upslope lip of the tray (i.e. opposite the runoff outlet) to avoid a windward edge effect during WDR events. This layer extended over the full tray width and had a variable thickness along the tray length, as required to maintain a continuous soil surface flush with both the upslope edge and the runoff outlet, forming a wedge-shaped surface layer with a slight slope of 5 %. Each erosion tray was put on a base made of a perforated steel sheet covered with voile, which allowed any infiltrated water to drain freely and reach the infiltrate outlet. The soil erosion trays were then prepared to simulate different soil surface conditions: 1) smooth surface and 2) rough surface, with mounds and depressions.

The smooth surface was obtained by flattening the upper layer of soil using the soil packer. On the other hand, the rough soil surfaces were created using a specialised tool that formed offset mounds and depressions of 2 cm height and depth, respectively, simulating non-directional surface roughness. The roughness was applied uniformly across the soil surface, ensuring consistency across replicates.

Soil trays were put in water that reached the trays' base, allowing the soils to wet up by capillary rise for a period of 24 h, after which they were removed from the water bath to allow them to drain. This resulted in a soil volumetric moisture of 42.66 % ± 0.21 (measured using Delta-T HH2/SM150T soil moisture probe), close to the expected saturated water content of 0.47 for a soil at this bulk density.

2.2. Calibration of the rainfall and wind simulators

2.2.1. Rainfall simulator

The erosion experiments were run indoors with rainfall and wind simulators (section 2.2.2) to avoid interference from external environmental factors such as natural wind or rainfall. The targeted rainfall intensity (90 mm hr^{-1}) and duration (30 min) were selected to simulate natural representative rainfall events. To achieve that, the pressurised water rainfall simulator was tested using water pressures ranging between 0.4 and 0.7 bar at a number of locations under the rainfall nozzle. The intercepted volume of water was measured using catch cups placed on a tilting table (set at the test slope gradient of 11 %). Each test was performed in triplicate. Once the approximate area and water pressure that delivered the desired rainfall intensity were identified, additional tests were carried out placing an empty erosion tray at different positions under the nozzle to determine locations of rainfall intensity uniformity for the erosion trays during the windless and wind-driven rainfall simulations.

The nozzle that produced the desired intensity was a LECHLER 490.888.30.CG, placed at 1.5 m above the soil surface, and at a 1-meter distance above the pressure gauge. The pressure was maintained at 0.5 bar. Catch cups were placed next to the erosion trays during each run to check for consistent rainfall application over space and time.

The Christiansen's coefficient of uniformity (CU, %) (Christiansen, 1942) was used to determine the spatial distribution of rainfall on the test area (i.e. erosion tray location). It is expressed in Equation (1), where x is the water collected in the catch can (mL), and m is the average water volume collected (mL).

$$CU = \left(1 - \frac{\sum |x - m|}{\sum x}\right) \cdot 100 \quad (1)$$

The Christiansen's coefficient was 98 %, indicating homogeneous distribution of rainfall on the soil surface. The trays were set on a slope gradient of 6.5 degrees (~11 %), to be representative of typical arable field conditions.

2.2.2. Wind simulator

A portable 3-phase electric wind simulator was used in combination with the rainfall simulator, an open-type system, to generate wind-driven rain (Fig. 1). The sloped erosion trays were oriented in the same direction as the generated wind. The wind simulator was calibrated to deliver wind velocities of 6 m s^{-1} and 10 m s^{-1} to the test area. In this study, two levels of wind-driven rain were simulated, hereafter

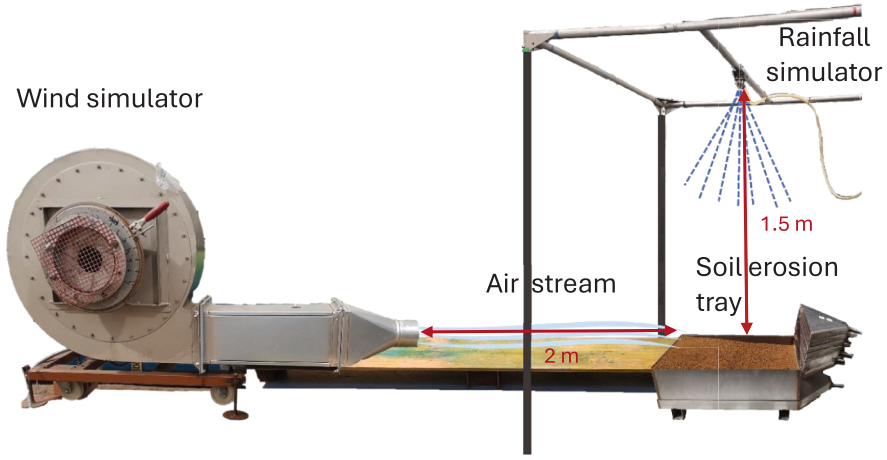

Fig. 1. Experimental setup combining wind and rainfall simulators, generating wind-driven rain (WDR) on a soil erosion tray.

named WDR1 (for the lower wind velocity, 6 m s^{-1}) and WDR2 (for the higher wind velocity, 10 m s^{-1}). Wind velocities were measured at different locations of the test area, where the erosion tray was placed, using a pre-calibrated hot wire anemometer (multicomp^{PRO}), considering different positions of the wind simulator. The position that delivered the desired wind characteristics was 2 m (horizontal) between the wind outlet and the erosion tray. A smooth wooden board (2.5 m long) was placed beneath the wind outlet and extended to the upslope edge of the erosion tray acting as a flow straightener by providing a continuous surface over which the airflow could stabilize, thereby ensuring a more uniform wind flow.

Fig. 2 shows the distribution of wind velocities over the length of the erosion tray. Three-dimensional wind velocity profiles (in x, y, z directions) were created at the two experimental wind velocities by measuring the wind velocity at different points across the width and along the length of the tray and at the following heights above the

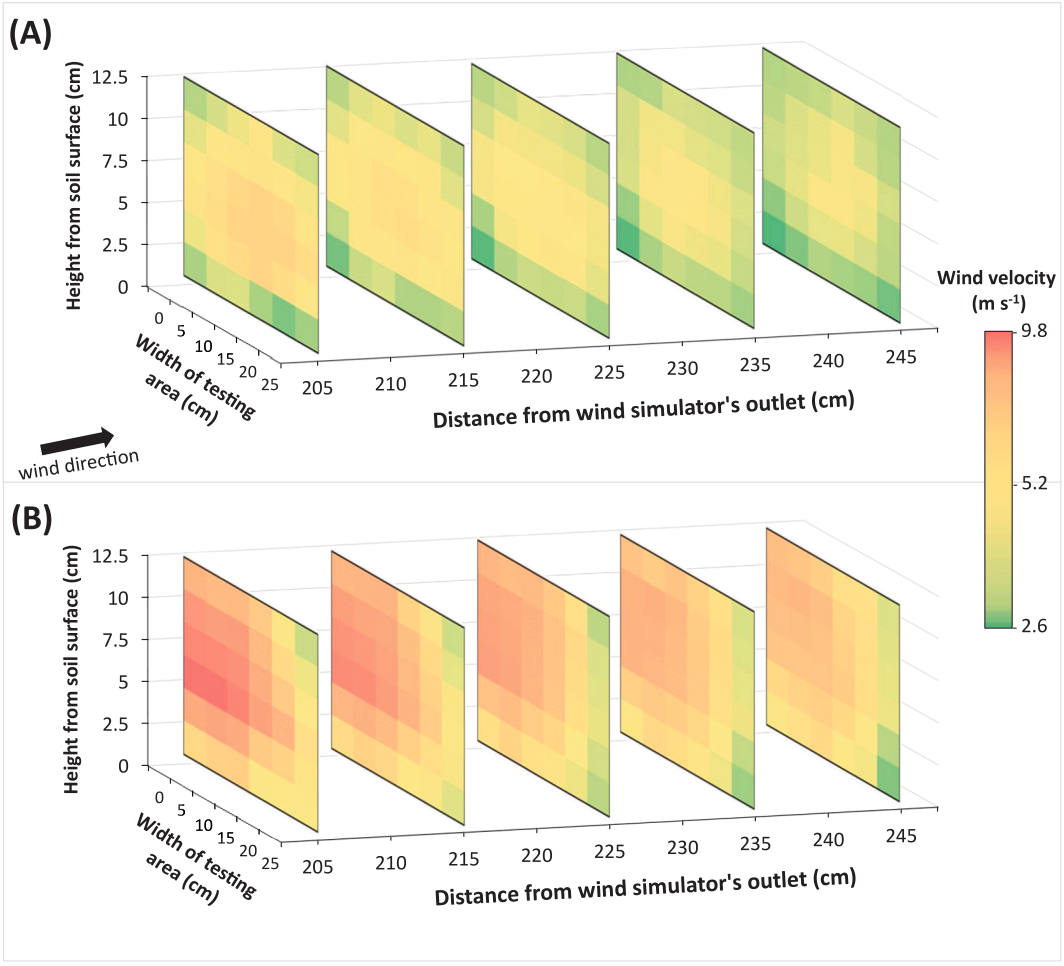

Fig. 2. Spatial distribution of the wind velocity (m s^{-1}) over the test area with (A) the lower wind velocity, used to simulate WDR1 and (B) the higher wind velocity, used to simulate WDR2.

erosion tray: 0 cm (at the soil surface), 2.5 cm, 5 cm, 7.5 cm, 10 cm, 12.5 cm. The number of measured points was 180 points per each wind velocity profile. Considering the vertical section of the test area located 2.05 m beyond the wind simulator's outlet (Fig. 2), the wind velocities at the middle of the section were 6 m s^{-1} and 10 m s^{-1} in the two wind configurations simulating WDR1 and WDR2, respectively.

The spatial distribution of wind-driven rainfall on the test area was measured using the uniformity method described in section 2.2.1., and the average Christiansen uniformity coefficients were 97 % for WDR1 and 96 % for WDR2, indicating that the wind-driven rainfall maintained a high level of spatial uniformity across the test area.

2.2.3. Windless (WLR) and wind-driven rainfall (WDR) kinetic energy (KE)

Rainfall erosivity refers to the rainfall's ability to detach, entrain and transport soil particles, and is crucial for understanding erosion processes (Nearing et al., 2017). It is quantified through the total cumulative KE of an individual rainfall event, which depends on the raindrop distribution and raindrop mass and velocity.

The size, frequency (number of detected raindrops per unit time), vertical velocity of raindrops and their angle of incidence were measured using the high-performance Oxford Laser VisiSize N60 at Silsoe Spray Unit Applications (Silsoe, UK). The equipment uses a short dual light pulse to illuminate a screen, capturing images where droplets are visible as dark spots against a light background. The images are then analysed using the VisiSize software (Oxford lasers). The laser, rainfall simulator nozzle and wind generator were set up to replicate the same distances and heights between the test area and the rainfall/wind sources as in the experimental setup described above. The water pressure, water flow rate, and wind velocities were also replicated in the same way. The laser was positioned at two different sampling locations under the rainfall simulator nozzle: i) central (location 1) and ii) at 25 cm from the vertical line to the nozzle, away from the wind source (location 2). The measurements were repeated five times for each of the two locations and for each of the three treatments (WLR, WDR1 and WDR2).

The resultant velocity (v, m s^{-1}) of windless and wind-driven raindrops was calculated from the measured vertical velocity (V_v, m s^{-1}) and the raindrop angle of incidence (α, deg) in Eq. (2).

$$\boldsymbol{v} = \frac{1}{\boldsymbol{cos\alpha}} \cdot \boldsymbol{V_v} \tag{2}$$

The resultant kinetic energy (KE_r, mJ) of the windless and wind-driven raindrops was calculated using Eq. (3), where m is the mass of the raindrop (g).

$$\boldsymbol{KE_r} = \frac{1}{2}\boldsymbol{m} \cdot \boldsymbol{v}^2 \tag{3}$$

The kinetic energy (KE, mJ m^{-2} s^{-1}) is defined in Eq. (4), where ρ is the density of water (g cm^{-3}), D is the diameter of the raindrop (cm), and n is the number of detected raindrops falling in each drop diameter and velocity per unit area per unit time.

$$\boldsymbol{KE} = \left(\frac{\boldsymbol{\pi}}{12}\right) \cdot \boldsymbol{\rho} \cdot \boldsymbol{D}^3 \cdot \boldsymbol{n} \cdot \boldsymbol{v}^2 \tag{4}$$

The total kinetic energy per unit area and time is the sum of all KE calculated for each drop diameter (mm) and velocity (m s^{-1}).

2.3. Measurements of erosion and soil surface roughness

2.3.1. Runoff, infiltration, sediment load and concentration

The measurements followed the methodology described in Bahddou et al. (2023). For each erosion tray, total volumes of surface runoff and infiltrate were collected after 30 min of the experimental run from the tray's outlet and the base's outlet respectively, via a system of pipes and buckets, and measured using measuring cylinders. The time taken for runoff and infiltrate initiation (seconds) was recorded. The mass of sediments collected in the runoff was also recorded after the 30-minute events. When the runoff volume was less than 100 mL, the total collected volume was filtered through oven-dried, pre-weighed Whatman Number 2 filter paper. When the runoff volume was greater than 100 mL, the total mixture was thoroughly agitated, and a sub-sample of 100 mL was taken and filtered. The sediment-loaded filter papers were oven-dried for 24 h at 105 °C and weighed using a precision balance with a readability of 0.001 g. The sediment concentration in the runoff (g L^{-1}) was then calculated.

2.3.2. Rainsplash erosion

Rain-splashed material was collected by placing purpose-designed collectors at the downslope end of the erosion tray, right on top of the runoff outlet funnel. The collectors covered the whole width of the erosion tray and were designed to collect the detached and transported soil particles (due to WLR and WDR) at different heights (0–2.7 cm; 2.7–5.4 cm; 5.4–7.1 cm; 7.1–8.8 cm; 8.8–10.5 cm; and 10.5–12.2 cm) above the erosion tray surface (Fig. 3). Plastic bottles were placed at the end of each collector to capture any potential soil particle that was further transported by wind inside each collector.

The sediment-loaded funnels and bottles were rinsed to collect all the soil particles, which were quantified following the sediment processing procedure described in section 2.3.1.

2.3.3. Soil surface roughness (SSR)

Soil surface roughness was measured before and after the WLR and WDR events to assess the comparative effect of WLR and WDR and runoff on the soil surface morphology during the different three events (WLR, WDR1 and WDR2). For this, soil surfaces were scanned at 1.5 mm resolution using a laser scanner (Creaform EXAscan 3D Handscanner), along with VXelements, an integrated 3D scanning software. The scans were converted to the appropriate format and processed using Geomagic Studio® software, then the 3D surface areas were computed to obtain a calculated 3D surface area. The soil surface roughness (SSR, %) was calculated using Eq. (5), where A is the plane surface of the soil tray (mm^2), and S is the actual area of the soil surface with its microtopographic irregularities (mm^2).

$$\boldsymbol{SSR} = \frac{(\boldsymbol{S} - \boldsymbol{A})}{\boldsymbol{A}} \cdot 100 \tag{5}$$

2.4. Statistical analysis

The simultaneous effect of rainfall and wind on erosion processes under different soil surface conditions was investigated. The experiment involved three rainfall events (WLR, WDR1, WDR2), each applied to two soil surface conditions (smooth and rough), with four replicates per combination, resulting in 24 erosion trays. It was a split plot design with a factorial treatment structure; the WLR, WDR1 and WDR2 treatments were randomised to pairs of trays and smooth vs rough surfaces were randomised to individual trays within each pair. The data obtained from the measurements was subjected to ANalysis Of VAriance (ANOVA) using the statistical software Genstat® (22nd Edition). A pairwise comparison of the means was performed for the significant cases (with a p-value < 0.05) using the Least Significant Differences (LSDs) at the 5 % level of probability. Residual plots were assessed to determine the appropriate scale for analysis. To meet statistical assumptions, a LOG transformation was applied to the sediment load and splash erosion data, while a square root (SQRT) transformation was performed for the sediment concentration data.

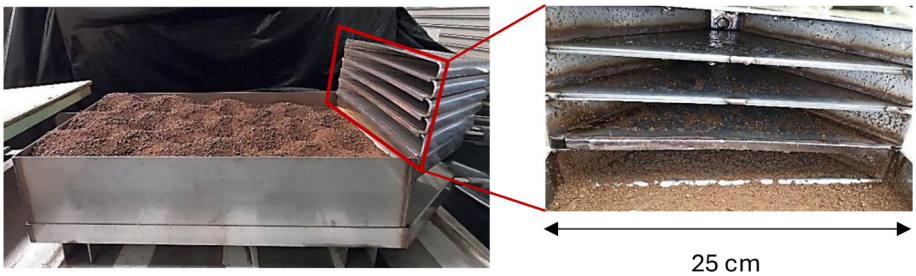

Fig. 3. An erosion tray with a set of collectors downslope collecting the detached soil particles by rainsplash due to windless and wind-driven rainfall.

3. Results

3.1. Windless (WLR) and wind-driven rainfall (WDR) kinetic energy (KE)

As expected, the raindrops' angle of incidence increased with increasing wind velocity (Fig. 4). The angles of incidence > 50° correspond to raindrops < 0.5 mm in diameter under WDR1, because the smaller the raindrop, the more its trajectory is influenced by wind. Under the highest wind velocity, WDR2, raindrops of up to 1 mm in diameter were inclined at 50° to 80° from the vertical. This aligns with the findings of Sharon (1980) who reported that angles of 40° to 70° have been recorded in rainfall driven by a wind velocity of 10 m s^{-1}.

The vertical raindrop velocities were higher during WLR than during WDR conditions. This is because under WLR, the trajectory of the raindrops was vertical (i.e. perpendicular to the test area), whereas under WDR conditions, the angle of raindrop incidence increased, hence the vertical velocity decreased.

Table 1 depicts the differences between WLR, WDR1 and WDR2 in terms of the raindrop velocity and total KE. After considering the raindrop incidence angle (Equation (2)), the resultant velocity increased in WDR conditions compared to WLR, especially for WDR2 where it increased by 95 %. The KE also increased in WDR conditions compared to WLR, especially for WDR2 where it increased by 43.5 %.

Table 1
Vertical velocities, resultant velocities and resultant kinetic energies of windless and wind-driven rainfall measured by the VisiSize Laser positioned at two different locations under the nozzle. Mean values are presented.

	Windless and Wind-Driven Rainfall events		
	WLR	**WDR1**	**WDR2**
Vertical velocity (m s^{-1})	2.45	1.97	1.53
Resultant velocity (m s^{-1})	2.45	2.74	4.78
Total KE (mJ m^{-2} s^{-1})	313	360	449

3.2. Time-to-runoff initiation and runoff volume

Time-to-runoff initiation refers to the interval between the onset of rainfall and the generation of the initial outflow at the runoff outlet. Time-to-runoff initiation (seconds) was recorded for each erosion tray during both the windless rainfall (WLR) and wind-driven rainfall (WDR) simulations. There was a significant difference in time-to-runoff initiation between the three rainfall events (p = 0.003), ranked WDR2 < WDR1 < WLR for both the smooth and the rough surfaces, suggesting that the WDR events significantly reduced time-to-runoff initiation (i.e. speeded up the initial generation of runoff) compared to the WLR event.

For the smooth surface, time-to-runoff initiation (mean ± standard error) was 51 ± 4 s, 67 ± 5 s, and 103 ± 8 s for WDR2, WDR1 and WLR, respectively. For the rough surface, time-to-runoff initiation was 61 ± 10 s, 81 ± 7 s, and 150 ± 17 s for WDR2, WDR1 and WLR, respectively. During all events, the rough surface had significantly delayed runoff initiation compared with the smooth surface (p = 0.008), due to the mounds and depressions that make the path longer for runoff to reach the outlet.

Mean runoff volume (mL) varied significantly across the three rainfall events (p < 0.001). For the smooth surface, the runoff volume was ranked WLR < WDR1 < WDR2, while for the rough surface, the ranking was WDR1 < WLR < WDR2 (Fig. 5a). For the smooth surface, the runoff volume on WDR1 and WDR2 increased by 36 % and 74 % compared to the WLR condition, respectively. On the other hand, for the rough surface, runoff decreased by 49 % on the WDR1 event and increased by 15 % on the WDR2 event compared to the WLR condition. However, the LSDs at the 5 % level showed that there was no significant difference between WLR and WDR2 for the rough surface. The smooth surface generated runoff volumes that were 1.5, 4.1 and 2.3 times the volumes generated by the rough surface during the WLR, WDR1 and WDR2 events respectively.

3.3. Time-to-infiltrate initiation and infiltrate volume

Time-to-infiltrate initiation (seconds) is the period between the start

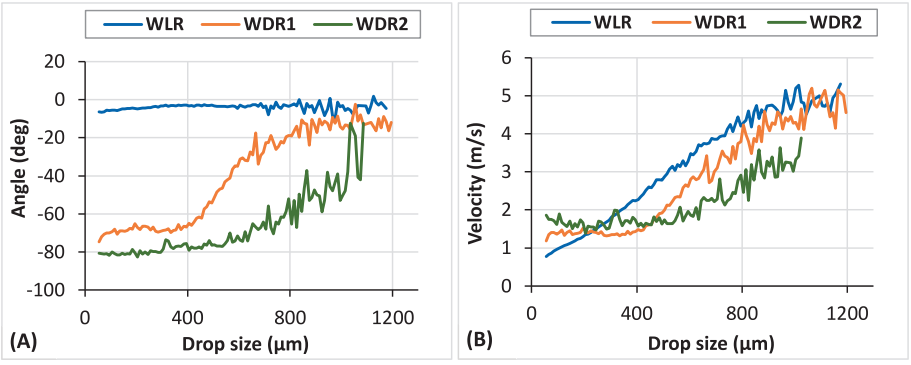

Fig. 4. (A) Raindrop incidence angle (deg) and (B) vertical velocity (m s^{-1}) at different raindrop sizes under WLR, WDR1 and WDR2. The data is the mean of both VisiSize Laser locations.

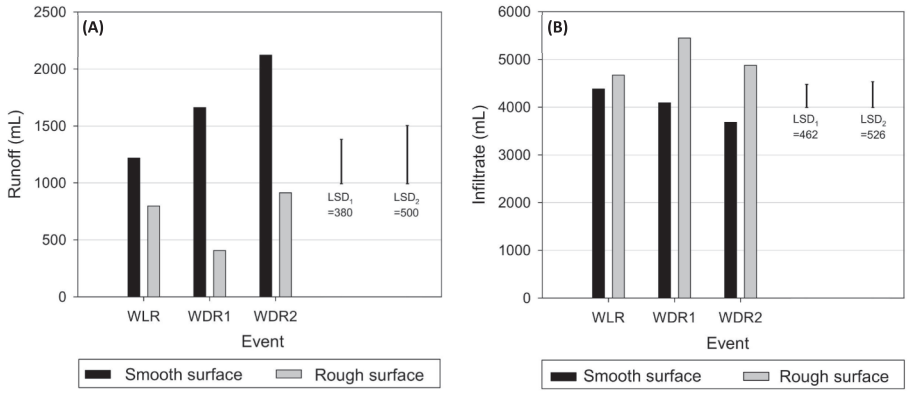

Fig. 5. (A) Mean runoff volumes (mL), and (B) mean infiltrate volumes (mL) generated during the three 30-minute events (WLR, WDR1 and WDR2) on smooth and rough surfaces. In both cases, the Event × Surface interactions are significant ($P < 0.05$); The LSD_1 bars apply to comparisons between the three rainfall events, while LSD_2 bars compare between the smooth and rough soil surfaces within an event.

of the rainfall and the generation of the first outflow at the infiltrate outlet. This was recorded for each erosion tray during all rainfall simulations (with and without wind). Infiltrate was always initiated before runoff ($p < 0.001$), where the mean value of time-to-infiltrate initiation was 36 ± 2 s, whereas the mean value of time-to-runoff initiation was 86 ± 8 s. Time-to-infiltrate initiation was not significantly influenced by rainfall events ($p = 0.92$), or SSR conditions ($p = 0.61$).

The infiltrate volume (mL) was significantly different between the three rainfall events ($p < 0.05$). The infiltrate volume was ranked WDR2 < WDR1 < WLR on the smooth surface. For the smooth surface, the infiltrate volume for WDR1 and WDR2 decreased by 7 % and 16 % compared to the WLR condition respectively. On the other hand, for the rough surface, WDR1 generated the significantly higher infiltrate volume, increasing it by 17 % compared to the WLR condition. There was no significant difference in infiltrate volume between WLR and WDR2 for the rough surface (Fig. 5b).

There was a significant difference in infiltrate volume between the different surface conditions ($p < 0.001$). The rough surface generated infiltrate that was 1.1, 1.3 and 1.3 times the volumes generated by the smooth surface during the WLR, WDR1 and WDR2 events respectively. As expected, there was a strong negative correlation between mean runoff volumes and mean infiltrate volumes ($r = -0.95$).

3.4. Sediment load and concentration in the runoff

Total sediment load in the runoff (mg) was measured under WLR, WDR1 and WDR2 for both soil surface conditions. The results indicate that WDR2 generated higher sediment loads than the WLR and WDR1, where mean values increased by 43 % for WDR2 compared to WLR on the smooth surface (Fig. 6a). There was a strong positive correlation between runoff volume and sediment load ($r = 0.74$), as soil particles were both detached and then entrained and transported by the runoff.

The sediment concentration in the runoff (g L^{-1}) was significantly higher for WDR2 than for the two other events (it increased by 143 % for WDR2 compared to WLR). This result is valid only for the smooth surface. For the rough surface, there was no significant difference in sediment concentration between WLR, WDR1 and WDR2. The difference in sediment concentration between the smooth and rough surfaces was significantly different under WDR2 (Fig. 6b).

3.5. Splash erosion by windless (WLR) and wind-driven rainfall (WDR)

The significantly highest mean splash erosion (mg) for all treatments was recorded by the sediment collector with the height range 0–2.7 cm above the soil surface. Splash erosion at this height range was ranked WLR < WDR1 < WDR2 on the smooth surface, and WDR1 < WLR < WDR2 on the rough surface. There was a significant difference between

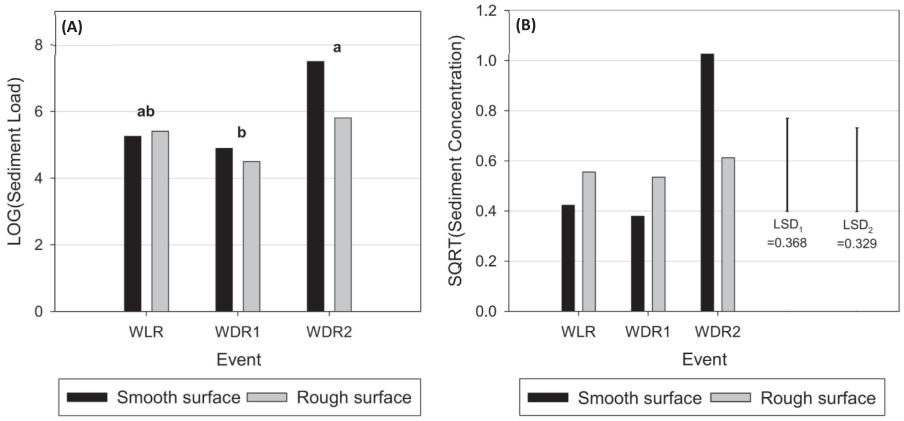

Fig. 6. (A) Log-transformed mean total sediment load (mg), and (B) Square-root-transformed mean sediment concentration in the runoff (g L^{-1}), generated during the three 30-minute events (WLR, WDR1 and WDR2) on smooth and rough surfaces. In (A), the Event × Surface interaction and Surface main effect are not significant ($P > 0.05$); Different lowercase letters above bar pairs indicate significant differences between the Rainfall Event main effect ($P < 0.05$) based on the $LSD_{Event} = 1.511$. In (B), the Event × Surface interaction is significant; The LSD_1 bar applies to comparisons between the three rainfall events, while the LSD_2 bar compares between the smooth and rough soil surfaces within an event.

the three rainfall events and between the six height ranges for sediment collection ($p < 0.001$). The splash erosion under the WDR2 event was significantly greater, at all heights, than that under the WLR and the WDR1 (Fig. 7). This was the case for both rough and smooth surfaces.

3.6. Effect of windless (WLR) and wind-driven rainfall (WDR) on initial soil surface roughness (SSR)

Table 2 presents the initial and final SSR of the smooth surface (hereafter referred to as 'SS') and the rough surface (hereafter referred to as 'RS') after the three different rainfall events (WLR, WDR1 and WDR2). The initial SSR of the rough surface was higher than the initial SSR measured for the smooth surface ($p < 0.001$).

As expected, the SSR of the initially smooth surface significantly increased after each rainfall event. This increase in SSR was significantly different between all three events ($p < 0.05$) and was ranked WDR2 > WDR1 > WLR (Fig. 8). On the other hand, the SSR of the initially rough surface declined after each rainfall event. This decline was more pronounced after the WDR events (WDR2 > WDR1 > WLR). The final SSR after the three events remained significantly different between the two surface conditions ($p < 0.001$) and was significantly different from the initial SSR for both surface conditions.

For the initial rough surface (prior to rainfall), the mounds and depressions created areas of both light and dark (i.e. illumination and shadow) as shown in Fig. 9. It is clearly noticeable that the light tone gets more extensive, and the dark shadow gets lighter after applying WLR and WDR, which indicates the reduction in the magnitude of mounds and depressions. For the smooth surface, after the simulated WLR and WDR events, small pits were formed due to the raindrop impact that led to soil detachment and concomitant compaction. This is represented by the contrast of tones (light vs dark) in Fig. 9.

4. Discussion

4.1. Windless (WLR) and wind-driven rainfall (WDR) kinetic energy (KE)

An important aspect of wind is that it alters the KE of raindrops falling onto the soil. The increase in the KE in WDR conditions, especially for WDR2, compared to WLR (as shown in Table 1), was attributed to the increase in the resultant velocity. This aligns with the results of Erpul et al. (2003a; 2005; 2008; 2009). The effect of wind on the rainfall

Table 2
Soil surface roughness (SSR, %) for smooth (SS) and rough (RS) surfaces, before (initial SSR) and after (final SSR) the three 30-minute events (WLR, WDR1 and WDR2).

Treatments	Surface roughness (%)	
	Before rain	After rain
SS-WLR	4.19	7.29
SS-WDR1	3.1	6.72
SS-WDR2	3.33	9.05
RS-WLR	20.19	16.55
RS-WDR1	24.58	19.25
RS-WDR2	24.89	17.48

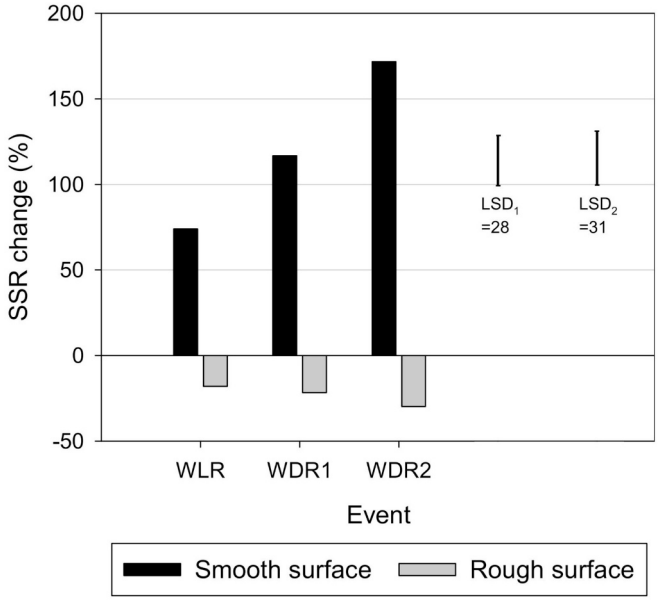

Fig. 8. Changes in the Soil Surface Roughness (SSR, %) for the two surface conditions during the WLR, WDR1 and WDR2 events. The Event × Surface interaction is highly significant ($P < 0.001$); The LSD_1 bar applies to comparisons between the three rainfall events, while the LSD_2 bar applies to comparisons between the smooth and rough soil surfaces within an event.

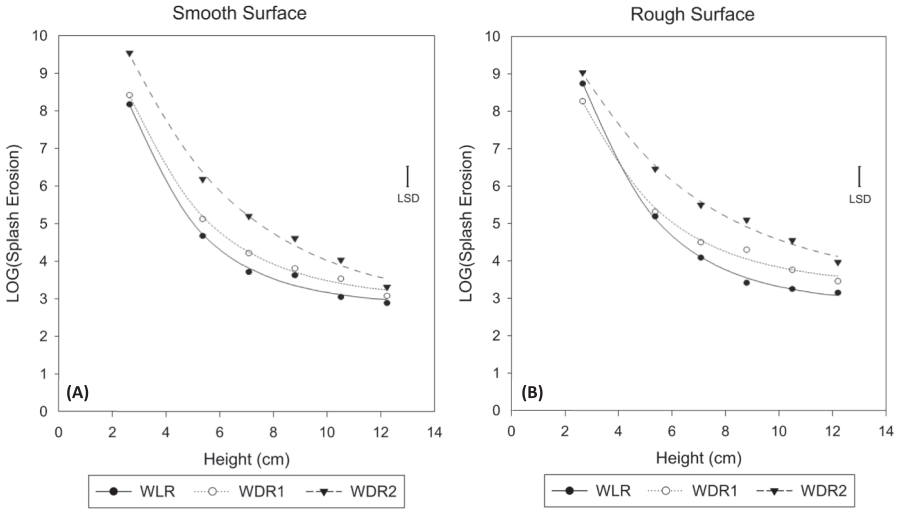

Fig. 7. Log-transformed mean total splash erosion (mg) generated during the three 30-minute events (WLR, WDR1 and WDR2), collected at different heights above the (A) smooth and (B) rough soil surfaces. The Height × Event × Surface interaction is significant ($P < 0.05$); The LSD bar (= 0.514) compares either different rainfall events at a given height, or different heights within the same event, across both panels (A) and (B).

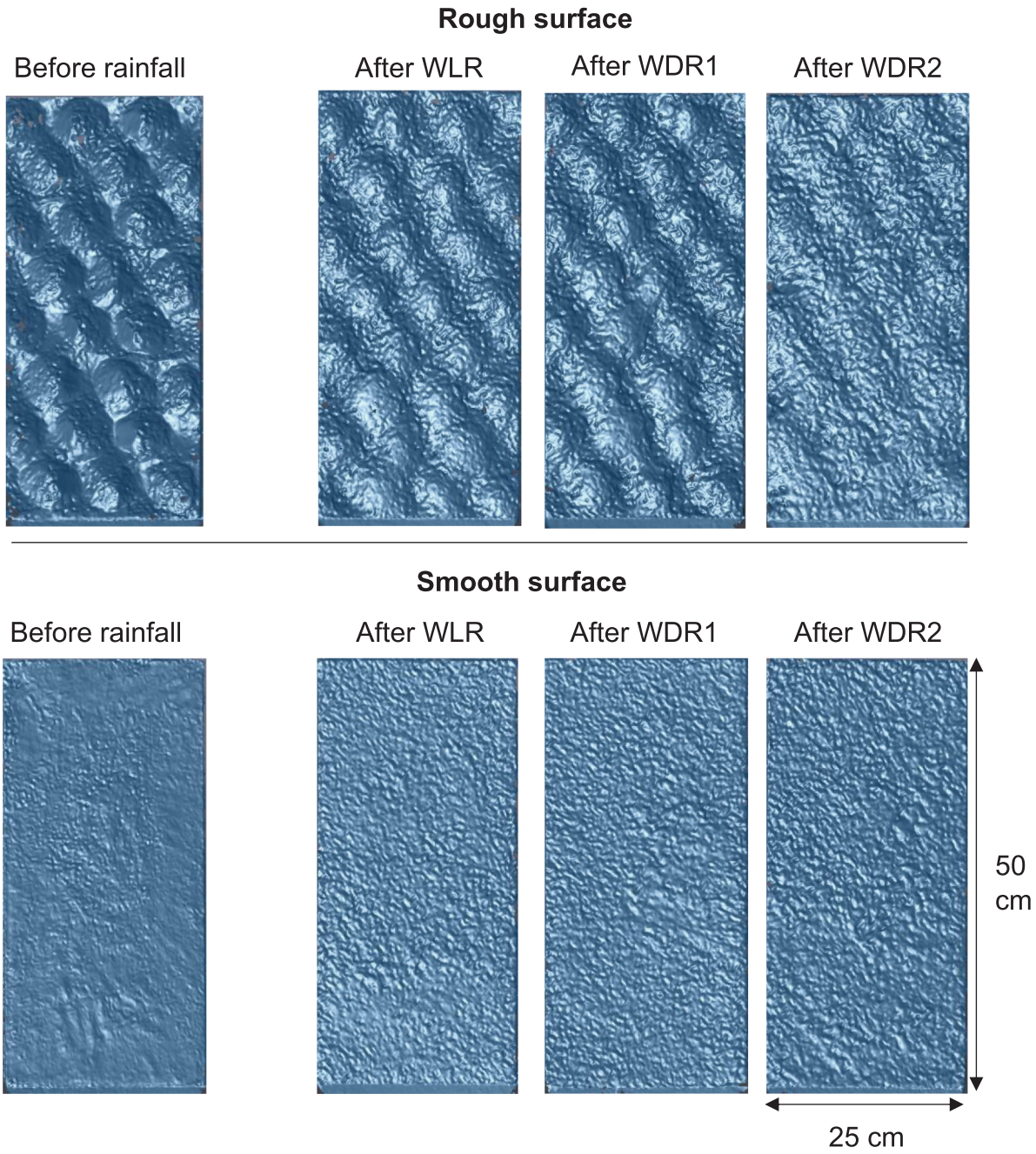

Fig. 9. Changes in the soil surface of the initially smooth and rough surfaces before and after windless rain (WLR), wind-driven rain1 (WDR1) and wind-driven rain2 (WDR2). Images are from a laser scanner with a resolution of 1.5 mm. Each image represents the erosion trays' dimensions of 50 cm × 25 cm.

KE depends on whether the vertical or the resultant fall velocity is considered (Tilg et al., 2020). Tilg et al. (2020) found that rainfall KE decreased with increasing wind speed and explained this result by considering the vertical fall velocity of raindrops only. This underestimates the effect of the wind on raindrop erosivity. Therefore, the raindrop incidence angle is important when determining the overall KE. Results from other studies may also vary due to the apparatus used. Kim and Song (2018) used a Parsivel disdrometer which is not ideal under windy conditions because of the dispersion and deviation of raindrops which affect drop size distribution and fall velocity. Also, that device does not measure raindrop incidence angle and misclassification of raindrop characteristics could occur due to raindrops not falling perpendicular to the test area (Friedrich et al., 2013).

4.2. Runoff, infiltration, sediment load and concentration

For the initially smooth surface, runoff volumes were positively correlated with wind velocity, and sediment load and concentration increased under the WDR2 event as compared with WLR and WDR1. This is in accordance with the findings of Erpul et al. (2003b) and An et al. (2023), where wind-driven runoff detached, entrained and transported more soil particles under higher wind velocities, leading to greater soil loss. Compared to windless rainfall, the wind affected the characteristics of the incoming rainfall (Erpul et al., 2013; Arshad et al., 2019) by altering the raindrops' trajectories, increasing their incidence impact (Gao et al., 2021). This alteration resulted in stronger tangential shear stress from the inclined rainfall (Erpul et al., 2005) which added momentum to the surface runoff, increasing its erosivity (i.e. capability

to detach and transport soil material (Iserloh et al., 2013)). Previous research reported that because of increased incidence angle and KE due to increased drop velocities, wind-driven rainfall may be more erosive, enhancing both soil detachment and transport (Erpul et al., 2008; Arshad et al., 2019).

Contrary to these findings, for the rough surface in the present study, surface runoff volumes significantly decreased under WDR1 compared with WLR. Under low wind velocities, it was observed that WDR on rough surfaces tended to create a more irregular flow pattern compared to windless rain. This can be explained by air turbulence associated with the roughness of the soil surface. In addition to that, wind velocities decrease near the ground surface when roughness is present (Morgan & Rickson, 1995). This decrease in wind velocity is more marked with increasing distance away from the air source (Fig. 2). The interception of WDR by surface mounds investigated in this study might cause water to be diverted or redistributed across the soil surface, leading to a more diffuse distribution of water and potentially less concentration of surface runoff. Moreover, the presence of mounds and depressions disrupted the flow of water, causing it to pool in low-lying areas and infiltrate into the soil rather than flowing over the surface as runoff. The interrupted flow paths and temporary water storage in depressions decreased both the velocity and the volume of surface runoff.

Under WDR2, runoff and soil loss on the rough surface increased compared to WDR1, to reach values not significantly different from those under WLR. When wind velocity increases to a certain threshold (e.g. 9 m s^{-1} according to Arshad et al. (2019)), the dynamics of soil erosion can change, potentially leading to runoff and soil loss levels similar to, or even higher than, those observed under windless rain conditions. Higher wind velocities during a wind-driven rain event (i.e. WDR2) might change the surface roughness by flattening the mounds (Fig. 9), leading to increased runoff compared to WDR1, which explains the significant difference between these two events. In addition to that, the mounds and depressions of the rough surface treatment simulated both windward and leeward slopes. Unlike the leeward slope where wind increases runoff and soil loss, under windward conditions, wind decreases runoff because raindrops fall at an obtuse angle to the slope and are incident in the opposite direction to the soil surface overland flow (An et al., 2022; 2023). This allows more time for the water to infiltrate, reducing runoff generation, so mitigating the erosive impact of water flow. The effects of both windward and leeward slopes (i.e. mounds and depressions) counterbalanced each other, which might explain the non-significant difference between WLR and WDR2 in terms of runoff volume and soil loss.

The rough surface (RS) delayed the time-to-runoff initiation and generated lower runoff volumes than the smooth surface (SS) for all rainfall events, and this decrease in runoff volume due to RS was highly significant for WDR1 and WDR2. The depressions on the rough surface retained the water during the rainfall event, which increased the infiltrate volume and delayed the time-to-runoff initiation compared to the smooth surface. This aligns with the findings of Zhao et al. (2019; 2021). Moreover, rough surfaces after tillage disturbance have a reduced bulk density in the upper layer of the soil and increased soil porosity, so promoting higher infiltration (Sun et al., 2009). At the same time, rough surfaces increase the effective slope length compared with smooth surfaces which delays the arrival of overland flow at the bottom of the slope (Zhao and Wu, 2015). This effect is caused by the mounds on the surface creating a physical barrier to the downslope movement of the runoff. Salem et al. (2014) found that such surfaces could reduce runoff volumes by 61 %. Our results demonstrate that surface runoff volume in RS decreased by 58 % compared with SS. Sediment load also diminished in correlation with runoff volume reduction. In examining the impact of surface microrelief on soil erosion, Wu et al. (2016) suggested that the spatial structure of the surface microrelief has an important effect on the transportability of sediment. This type of surface roughness mimics reservoir tillage, which is used in some countries as a method for soil and water conservation (Zhao et al., 2021).

4.3. Rainsplash erosion

Soil erosion is a process that starts with the detachment of soil particles mainly due to raindrop impact (Morgan, 2005; Kinnell, 2005). The hypothesis being tested was that the interaction of wind with falling raindrops would enhance the process of soil detachment and transport by increasing raindrops' momentum, fall velocity and kinetic energy. All these properties are associated with higher rainfall erosivity (Arshad et al., 2019).

For eroded material collected at the first height (i.e. 0–2.7 cm above the soil surface), the hypothesis was accepted for the SS. However, for the RS, splash erosion decreased under WDR1 (although not significantly so). As previously stated, under the WDR1 event, the non-uniform flow patterns and temporary storage of surface water within depressions may have attenuated the velocity of water flow, so reducing the erosivity of surface runoff and associated soil loss. Nevertheless, for splashed material collected at all heights from 2.7 to 12.2 cm above the soil surface, the hypothesis could be accepted. Indeed, the results show an increase in splash erosion during the WDR events compared to the WLR event at these collecting heights, for both the SS and the RS. This increase was positively correlated with wind velocity. According to Zumr et al. (2020), there is a linear relationship between the amount of detached soil material and the rainfall KE. Indeed, our results demonstrate that the higher wind velocity (WDR2) generated more splashed material due to the increase in the erosivity of raindrops. This was also reported by Arshad et al. (2019) and Cornelis et al. (2004). Mahmoodabadi et al. (2021) noted that raindrops' size and angle of incidence both increased with higher wind velocities which then contributed to a higher detachment rate. In the absence of wind during rainfall, raindrops falling vertically result in particle movement in all directions. Conversely, in wind-driven rains, particle movement becomes more unidirectional, aligning with the prevailing wind direction, as outlined by Erpul et al. (2003b). Due to the momentum given to the falling drops by the wind, WDR increases the rainfall velocity and thus KE to detach, entrain and transport soil particles. Moreover, the wind shear velocity has the potential to entrain soil particles into the air flow (de Lima et al., 1992). Once the mass of an entrained particle exceeds the transport capacity of the airflow, the particle drops to the ground under gravity. As it falls, it bombards other soil particles, imparting its kinetic energy to them. In turn, those particles are detached and entrained into the airflow (Marzen et al., 2017). In the same context, the wind increases the transport of soil particles already entrained by this rainsplash-saltation process (Cornelis and Gabriëls, 2004).

At all heights $>$ 2.7 cm above the soil surface, the rough surfaces generated more splash erosion than the smooth surfaces under both WLR and WDR. The differences in splash erosion between these surface treatments are probably linked to the spatial configurations of the surface microrelief. Rainsplash erosion increases with increasing surface microrelief (Bullard et al., 2018). This is attributed to the increased soil surface area exposed to raindrops, facilitated by the presence of mounds and depressions (Luo et al., 2018). Microrelief on rough surfaces increased the effective slope lengths (and the soil surface area subjected to the rainfall and wind when present), leading to higher detachment rates (Wu et al., 2016).

4.4. Effect of windless (WLR) and wind-driven rainfall (WDR) on initial soil surface roughness (SSR)

Post-rainfall changes in SSR are primarily influenced by the initial state of the soil surface (Huang and Bradford, 1992; Magunda et al., 1997; Govers et al., 2000). Rainfall significantly changes soil surface morphology (Zhao and Wu, 2015) by decreasing or increasing SSR over the rainfall event. Our results indicate that the initially smooth surface became rougher after the WLR and WDR events, as raindrop impacts detached and (re)deposited soil particles. This aligns with the findings of Bahddou et al. (2023) where after detachment, particles were

transported and deposited on the soil surface, forming a new microrelief, leading to an increase in the SSR for initially SS. In this context, Zhao et al. (2014a) observed that on SS, distinct crescent-shaped pits formed after rainfall which increased their surface roughness. Likewise, Römkens et al. (2001) reported similar changes in surface roughness with rainfall, as a result of the development of rills and flow incisions.

Our results also show that there was a decrease in the SSR of the initially rough surfaces. This agrees with the findings of Zhao et al. (2014b) who found the initial SSR of a rough soil surface decreased by 23 % after rainfall. Detached soil particles from the mounds on the rough surface were transported to and deposited in lower points and surface depressions, which reduced the magnitude of mounds and depressions, leading to a decrease in the SSR. This was also reported by Kirkby (2001) and Zhao et al. (2019).

Our findings show that the initially smooth surface SSR increased by 74 % after WLR and by 117 % and 172 % after WDR1 and WDR2 respectively. The difference between these changes in SSR was significant. Although the changes in SSR for the rough surface were not significantly different for the three rainfall events, the pattern was the same as for the smooth surface, i.e. the decrease in SSR was more notable for the WDR events. As wind exerts an additional force on rainfall, raindrop erosivity and associated soil detachment, transport and deposition are increased. The wind also enhances the momentum and shear force of surface runoff. As a result of these two processes, the change in SSR during wind-driven events was escalated.

5. Conclusions

This study investigated the combined effect of wind and rainfall on soil erosion processes, addressing a key limitation in assessing erosion dynamics when both erosion agents operate simultaneously. These experiments directly compared windless and wind-driven rainfall events (with varying wind velocities) over smooth and rough surfaces, using purpose-designed erosion trays to measure surface runoff and infiltrate volumes, sediment load and concentration in the runoff, along with a set of funnels built as rainsplash sediment collectors. This study was unique in evaluating how rainfall erosivity interacts with soil surface roughness (SSR) under varying rainfall conditions.

The outcome of this research showed that, on initially smooth surfaces, wind-driven rainfall, WDR, increased surface runoff and soil losses compared to windless rainfall (WLR) with stronger effects at higher wind velocity (WDR2). This response reflects the increased rainfall erosivity due to increased rainfall resultant velocity and kinetic energy generated by the added horizontal wind component, which enhances raindrop impact and soil particle detachment. In contrast, initially rough surfaces reduced runoff and soil loss under low wind velocity (WDR1), but this mitigating effect was cancelled out under WDR2, resulting in soil and water losses comparable to or exceeding those observed under WLR. On the other hand, wind-driven rain enhanced changes in soil surface roughness (i.e. the increase and decrease in the SSR for the smooth and rough surfaces respectively), to a greater extent than seen for WLR events.

The results show that a rough surface delayed the time-to-runoff initiation and generated less runoff and more infiltrate than the smooth surface, under the three events: WLR, WDR1 and WDR2. This is due to impedance of runoff by surface mounds (associated with the rough surface) that created a physical barrier to downslope water movement, and depressions that retained surface water. However, rough surfaces presented relatively a larger exposed surface area to raindrop impact, making it more susceptible to splash erosion compared to the smooth surface.

The findings of this study confirm that wind affects the rainfall erosivity, soil erosion processes and evolution of SSR. It is important that these effects are considered in erosion studies to accurately evaluate soil and water losses, especially in regions exposed to wind-driven rainfall.

CRediT authorship contribution statement

Sophia Bahddou: Writing – review & editing, Writing – original draft, Visualization, Validation, Resources, Project administration, Methodology, Investigation, Formal analysis, Data curation, Conceptualization. **Wilfred Otten:** Writing – review & editing, Validation, Supervision, Resources, Project administration, Funding acquisition, Conceptualization. **W. Richard Whalley:** Writing – review & editing, Visualization, Funding acquisition, Conceptualization. **Ho-Chul Shin:** Writing – review & editing, Funding acquisition. **Mohamed El Gharous:** Writing – review & editing, Funding acquisition. **Adnane Beniaich:** Writing – review & editing. **Hannah V. Cooper:** Writing – review & editing. **R. Jane Rickson:** Writing – review & editing, Validation, Supervision, Resources, Project administration, Funding acquisition, Conceptualization.

Declaration of competing interest

The authors declare that they have no known competing financial interests or personal relationships that could have appeared to influence the work reported in this paper.

Acknowledgments

This research is part of the PhD project FP03 entitled "Technical and practical innovations to reduce soil and water losses by improving soil physical properties". This project is within the "Sustainable Agriculture For Africa (SAFA)" programme which is a collaboration between Cranfield University, Rothamsted Research and Mohammed VI Polytechnic University. We would like to acknowledge OCP Group Morocco, the funder of this project, for its financial support. We appreciate Mr Cristinel Putinica and Ms Ceri Dawson from Cranfield University for their assistance with equipment setup and logistics, and Ms Jess Hood from Rothamsted Research for her feedback on the statistical analysis. We would like to acknowledge the Silsoe Spray Unit Applications team for providing the wind simulator and for their assistance in using the Oxford Laser VisiSize N60 to measure the raindrops characteristics. We also thank the UK Agri-Tech Centre, funded by Innovate UK, for the use of their facilities to conduct part of this research.

Data availability

The underlying data is accessible at doi.org/10.57996/cran.ceres-2824.

References

An, M., Han, Y., Zhao, C., Qu, Z., Xu, P., Wang, X., He, X., 2022. Effects of different wind directions on soil erosion and nitrogen loss processes under simulated wind-driven rain. Catena (Amst) 217, 106423. https://doi.org/10.1016/j.catena.2022.106423.

An, M., Wei, C.C., Han, Y., Qu, Z., Wang, X., Zhang, B., 2023. Soil erosion and nutrient loss due to changes in rainfall intensity under different wind directions. Earth Surf. Proc. Land. 1–13. https://doi.org/10.1002/esp.5674.

Arshad, R.R., Mahmoodabadi, M., Farpoor, M.H., Fekri, M., 2019. Experimental investigation of rain-induced splash and wash processes under wind-driven rain. Geoderma 337, 1164–1174. https://doi.org/10.1016/j.geoderma.2018.11.029.

Bahddou, S., Otten, W., Whalley, W.R., Shin, H.C., El Gharous, M., Rickson, R.J., 2023. Changes in soil surface properties under simulated rainfall and the effect of surface roughness on runoff, infiltration and soil loss. Geoderma 431, 116341. https://doi.org/10.1016/j.geoderma.2023.116341.

Bolan, S., Padhye, L.P., Jasemizad, T., Govarthanan, M., Karmegam, N., Wijesekara, H., Amarasiri, D., Hou, D., Zhou, P., Biswal, B.K., Balasubramanian, R., Wang, H., Siddique, K.H.M., Rinklebe, J., Kirkham, M.B., Bolan, N., 2024. Impacts of climate change on the fate of contaminants through extreme weather events. Sci. Total Environ. 909, 168388. https://doi.org/10.1016/j.scitotenv.2023.168388.

Bullard, J.E., Ockelford, A., Strong, C.L., Aubault, H., 2018. Impact of multi-day rainfall events on surface roughness and physical crusting of very fine soils. Geoderma 313, 181–192. https://doi.org/10.1016/j.geoderma.2017.10.038.

Christiansen, J.E., 1942. Irrigation by Sprinkling, Vol. 4. University of California, Berkeley.

Cornelis, W., Gabriëls, D., 2004. The effect of wind-driven rain on transport of sand by splash-saltation. In: Wind and Rain Interaction in Erosion. Wageningen University and Research Centre, pp. 129–142.
Cornelis, W.M., Oltenfreiter, G., Gabriels, D., Hartmann, R., 2004. Splash – saltation of sand due to wind-driven rain : vertical deposition flux and sediment transport rate. Soil Sci. Soc. Am. J. 68, 32–40. https://doi.org/10.2136/sssaj2004.3200.
da Rocha Junior, P.R., Bhattarai, R., Alves Fernandes, R.B., Kalita, P.K., Vaz Andrade, F., 2016. Soil surface roughness under tillage practices and its consequences for water and sediment losses. J. Soil Sci. Plant Nutr. 16, 1065–1074. https://doi.org/10.4067/S0718-95162016005000078.
de Lima, J.L.M.P., van Dijk, P.M., Spaan, W.P., 1992. Splash-saltation transport under wind-driven rain. Soil Technol. 5, 151–166.
Erpul, G., Gabriels, D., Cornelis, W.M., Samray, H., Guzelordu, T., 2009. Sand transport under increased lateral jetting of raindrops induced by wind. Geomorphology 104, 191–202. https://doi.org/10.1016/j.geomorph.2008.08.012.
Erpul, G., Gabriels, D., Cornelis, W.M., Samray, H.N., Guzelordu, T., 2008. Sand detachment under rains with varying angle of incidence. Catena (Amst) 72, 413–422. https://doi.org/10.1016/j.catena.2007.07.008.
Erpul, G., Gabriels, D., Norton, L.D., 2005. Sand detachment by wind-driven raindrops. Earth Surf. Proc. Land. 30, 241–250. https://doi.org/10.1002/esp.1178.
Erpul, G., Gabriels, D., Norton, L.D., Flanagan, D.C., Huang, C.H., Visser, S., 2013. Raindrop and flow interactions for interrill erosion with wind-driven rain. J. Hydraul. Res. 51, 548–557. https://doi.org/10.1080/00221686.2013.778339.
Erpul, G., Norton, L.D., Gabriels, D., 2003. The effect of wind on raindrop impact and rainsplash detachment. Trans. Am. Soc. Agric. Eng. 46, 51–62. https://doi.org/10.13031/2013.12548.
Erpul, G., Norton, L.D., Gabriels, D., 2003. Sediment transport from interrill areas under wind-driven rain. J. Hydrol. (Amst) 276, 184–197. https://doi.org/10.1016/S0022-1694(03)00070-2.
Erpul, G., Norton, L.D., Gabriels, D., 2002. Raindrop-induced and wind-driven soil particle transport. Catena (Amst) 47, 227–243. https://doi.org/10.1016/S0341-8162(01)00182-5.
Friedrich, K., Higgins, S., Masters, F.J., Lopez, C.R., 2013. Articulating and stationary PARSIVEL disdrometer measurements in conditions with strong winds and heavy rainfall. J. Atmos. Ocean Technol. 30, 2063–2080. https://doi.org/10.1175/JTECH-D-12-00254.1.
Gao, X., Yang, Z., Han, D., Gao, K., Zhu, Q., 2021. The impact of wind on the rainfall-runoff relationship in urban high-rise building areas. Hydrol. Earth Syst. Sci. 25, 6023–6039. https://doi.org/10.5194/hess-25-6023-2021.
Govers, G., Takken, I., Helming, K., 2000. Soil roughness and overland flow. Agronomie 20, 131–146. https://doi.org/10.1051/agro:2000114.
Helming, K., 2001. Wind speed effects on rain erosivity. Organization 771–776.
Huang, C., Bradford, J.M., 1992. Applications of a laser scanner to quantify soil microtopography. Soil Sci. Soc. Am. J. 56, 14–21. https://doi.org/10.2136/sssaj1992.03615995005600010002x.
Iserloh, T., Fister, W., Marzen, M., Seeger, M., Kuhn, N.J., Ries, J.B., 2013. The role of wind-driven rain for soil erosion - an experimental approach. Z. Geomorphol. 57, 193–201. https://doi.org/10.1127/0372-8854/2012/S-00118.
Kim, D.K., Song, C.K., 2018. Characteristics of vertical velocities estimated from drop size and fall velocity spectra of a Parsivel disdrometer. Atmos. Meas. Tech. 11, 3851–3860. https://doi.org/10.5194/amt-11-3851-2018.
Kinnell, P.I.A., 2005. Raindrop-impact-induced erosion processes and prediction: a review. Hydrol. Process. 19, 2815–2844. https://doi.org/10.1002/hyp.5788.
Kirkby, M., 2001. Modelling the interactions between soil surface properties and water erosion. Catena (Amst) 46, 89–102. https://doi.org/10.1016/S0341-8162(01)00160-6.
Luo, J., Zheng, Z., Li, T., He, S., 2018. Assessing the impacts of microtopography on soil erosion under simulated rainfall, using a multifractal approach. Hydrol. Process. 32, 2543–2556. https://doi.org/10.1002/hyp.13170.
Magunda, M.K., Larson, W.E., Linden, D.R., Nater, E.A., 1997. Changes in microrelief and their effects on infiltration and erosion during simulated rainfall. Soil Technol. 10, 57–67. https://doi.org/10.1016/0933-3630(95)00039-9.
Mahmoodabadi, M., Zamani, S., Yazdanpanah, N., 2021. Enrichment of soil organic carbon in the eroded sediments due to the simultaneous occurrence of rain and wind. Geoderma 386. https://doi.org/10.1016/j.geoderma.2020.114926.
Marzen, M., Iserloh, T., Casper, M.C., Ries, J.B., 2015. Quantification of particle detachment by rain splash and wind-driven rain splash. Catena (Amst) 127, 135–141. https://doi.org/10.1016/j.catena.2014.12.023.
Marzen, M., Iserloh, T., de Lima, J.L.M.P., Fister, W., Ries, J.B., 2017. Impact of severe rain storms on soil erosion: experimental evaluation of wind-driven rain and its implications for natural hazard management. Sci. Total Environ. 590–591, 502–513. https://doi.org/10.1016/j.scitotenv.2017.02.190.
Marzen, M., Iserloh, T., de Lima, J.L.M.P., Ries, J.B., 2016. The effect of rain, wind-driven rain and wind on particle transport under controlled laboratory conditions. Catena (Amst) 145, 47–55. https://doi.org/10.1016/j.catena.2016.05.018.
Morgan, R.P.C., 2005. Soil erosion and conservation, third ed. Blackwell Publishing Ltd.
Morgan, R.P.C., Rickson, R.J., 1995. Slope Stabilization and erosion Control: a Bioengineering Approach, first ed. E & FN SPON.
Nearing, M.A., Yin, S. qing, Borrelli, P., Polyakov, V.O., 2017. Rainfall erosivity: an historical review. Catena 157, 357–362. https://doi.org/10.1016/j.catena.2017.06.004.
Ries, J.B., Marzen, M., Iserloh, T., Fister, W., 2014. Soil erosion in Mediterranean landscapes - Experimental investigation on crusted surfaces by means of the Portable Wind and Rainfall Simulator. J. Arid Environ. 100–101, 42–51. https://doi.org/10.1016/j.jaridenv.2013.10.006.
Römkens, M.J.M., Helming, K., Prasad, S.N., 2001. Soil erosion under different rainfall intensities, surface roughness, and soil water regimes. Catena (Amst) 46, 103–123. https://doi.org/10.1016/S0341-8162(01)00161-8.
Salem, H.M., Valero, C., Muñoz, M.Á., Gil-Rodríguez, M., Barreiro, P., 2014. Effect of reservoir tillage on rainwater harvesting and soil erosion control under a developed rainfall simulator. Catena (Amst) 113, 353–362. https://doi.org/10.1016/j.catena.2013.08.018.
Sharon, D., 1980. The distribution of hydrologically effective rainfall incident on sloping ground. J. Hydrol. (Amst) 46, 165–188. https://doi.org/10.1016/0022-1694(80)90041-4.
Sun, Y., Lin, J., Lammers, P.S., Damerow, L., Hueging, H., Zhang, H., Sun, W., 2009. Predicting surface porosity using a fine-scale index of roughness in a cultivated field. Soil Tillage Res. 103, 57–64. https://doi.org/10.1016/j.still.2008.09.009.
Tilg, A.M., Vejen, F., Hasager, C.B., Nielsen, M., 2020. Rainfall kinetic energy in denmark: Relationship with drop size, wind speed, and rain rate. J. Hydrometeorol. 21, 1621–1637. https://doi.org/10.1175/JHM-D-19-0251.1.
Visser, S.M., Sterk, G., Ribolzi, O., 2004. Techniques for simultaneous quantification of wind and water erosion in semi-arid regions. J. Arid Environ. 59, 699–717. https://doi.org/10.1016/j.jaridenv.2004.02.005.
Wu, J., Zhao, L., Wu, F., Li, Z., 2016. The role of surface microreliefs in influencing splash erosion: a laboratory study. Soil Water Res. 11, 83–89. https://doi.org/10.17221/280/2014-SWR.
Zhang, H., Gao, Y., Sun, D., Liu, L., Cui, Y., Zhu, W., 2019. Wind erosion changes in a semi-arid sandy area, Inner Mongolia, China. Sustainability (Switzerland) 11. https://doi.org/10.3390/su11010188.
Zhao, L., Fang, Q., Hou, R., Wu, F., 2021. Effect of rainfall intensity and duration on soil erosion on slopes with different microrelief patterns. Geoderma 396, 115085. https://doi.org/10.1016/j.geoderma.2021.115085.
Zhao, L., Hou, R., Wu, F., 2019. Rainwater harvesting capacity of soils subjected to reservoir tillage during rainfall on the Loess Plateau of China. Agric Water Manag 217, 193–200. https://doi.org/10.1016/j.agwat.2019.02.048.
Zhao, L., Wu, F., 2015. Simulation of runoff hydrograph on soil surfaces with different microtopography using a travel time method at the plot scale. PLoS One 10, 1–14. https://doi.org/10.1371/journal.pone.0130794.
Zhao, L., Wu, J., Zhang, Q., Wu, F., 2014. Runoff, erosion and sediment particle size from smooth and rough soil surfaces under steady rainfall-runoff conditions. Acta Agric. Scand. B. Soil Plant Sci. 64, 623–632. https://doi.org/10.1080/09064710.2014.949297.
Zhao, L.S., Liang, X.L., Wu, F.Q., 2014. Soil surface roughness change and its effect on runoff and erosion on the Loess Plateau of China. J. Arid. Land 6, 400–409. https://doi.org/10.1007/s40333-013-0246-z.
Zumr, D., Mützenberg, D.V., Neumann, M., Jeřábek, J., Laburda, T., Kavka, P., Johannsen, L.L., Zambon, N., Klik, A., Strauss, P., Dostál, T., 2020. Experimental setup for splash erosion monitoring — study of silty loam splash characteristics. Sustainability 12, 157.

https://dspace.org/

Effect of wind-driven rain on soil erosion processes under different soil surface roughness conditions

Bahddou, Sophia; Otten, Wilfred; Whalley, W. Richard; Shin, Ho-Chul; El Gharous, Mohamed ...

2026-08
Elsevier
https://doi.org/10.1016/j.geoderma.2026.117908
Bahddou S, Otten W, Whalley WR, et al., (2026) Effect of wind-driven rain on soil erosion processes under different soil surface roughness conditions. Geoderma, Volume 472, August 2026, Article number 117908

Downloaded from a DSpace repository. https://dspace.org/